ESRF	**Experiment title:** Si/Ge mapping on sun micron scale of self-organized pits in strained epitaxial $Si_{1-x}Ge_x$ films on Si(001)	**Experiment number**: SI 623
Beamline: ID21	**Date of experiment**: from: 15/11/2000 to: 20/11/2000	**Date of report**: 01/03/2002
Shifts: 15	**Local contact(s)**: J. Susini	*Received at ESRF:*

Names and affiliations of applicants (* indicates experimentalists):

Luciana Di Gaspare, A. Notargiacomo, F. Evangelisti

Dip. Fisica, Universita' di Roma Tre, Via della Vasca Navale 84-00146 Roma Italy

E. Palange
Dipartimento di Energetica Università degli Studi di L'Aquila
67040 Monteluco di Roio – Italy

S. Pascarelli
European Synchrotron Radiation Facility

BP 220, 38043 Grenoble CEDEX – France

Report:

Deposition of high quality SiGe alloys on Si plays an important role for the fabrication of novel electronics and optoelectronic devices [1,2]. However it is well known that in heteroepitaxy the lattice mismatch between the different materials introduces defects like misfit dislocations, surface roughness and compositional non homogeneity that affect the device performances [3]. An interesting class of devices is based on the fabrication of modulation doped 2D electron gases (2DEG's) obtained by growing a strained Si channel buried between two relaxed SiGe layers [4-6]. One of these SiGe layers acts as a Virtual Substrate (VS) and the achievement of high electron mobility depends on the dislocation density of this relaxed SiGe film [7-9]. The best results are obtained when the VS is a compositionally graded SiGe buffer layer grown on a Si(001) surface followed by a thick layer at a fixed pre-set value. However the morphology of the sample surface presents waviness [10] and defects like pits [11-13]. The pits evolve during the VS growth following a self-organization mechanism that controls their nucleation and evolution [13]. The optimization of the

growth conditions results in a typical pit density less than 10 pits/cm^2. The observation that pits form even on few micron thick films, suggests that these defects are not simply related to impurities at the Si substrate/Si buffer interface.

In this paper we report on an X-ray Scanning Microscope (XSM) investigation of the Ge concentration variation inside the pits present in VS's. We will show that by mapping the Ge concentration with a spatial resolution of about 200 nm, we are able to elucidate the physical mechanisms of defect formation and evolution.

The VS's were grown by UHV Chemical Vapor Deposition at 700°C on top of Si buffer layers deposited at 850°C. The residual surface contamination was measured by X-ray photoelectron spectroscopy: the Si buffers and VS's were free from oxygen and carbon within the instrument sensitivity. The samples analyzed in this paper were compositionally graded VS's with a design similar to those used to fabricate high mobility 2DEG's [14]. The typical sample structure is constituted of a 500 nm thick Si buffer followed by 6 alloy layers (each 400 nm thick) having a step by step increasing Ge concentration with an average rate equal to 6.7%/μm. On top of the last layer a final 2.6 μm SiGe thick film was grown with a Ge concentration equal to 19%. Transmission electron microscopy in cross sectional view of a typical sample is reported in Fig.1. As we expect for relaxed VS's, misfit dislocations are present and concentrated at the Si/SiGe interface. The dislocations appear during the growth of the heterostructure for the need to relief the misfit strain and their presence guarantees the average relaxation of the sample. The image in Fig.1 does not evidence any localized region in which defects are concentrated. The good quality of the grown material is confirmed from the electrical transport properties of 2DEG's: we measured values of the electron mobility up to 10^5 Vcm^{2}s^{-1} [14].

In Fig.2 we report the optical microscope images and the atomic force microscope (AFM) profiles of two typical defects chosen for the XSM analysis. Pits A and B represent two stable phases in the evolution of the defect. During the growth of the VS, pit A evolves into pit B through a metastable phase (not reported here) represented by a pit having an octagonal shaped base [13]. Pit A is the initial stage of the pit evolution with the base-perimeter sides oriented along the [100] directions. Its morphological evolution is pit B having the base-perimeter oriented along the [110] directions. From the AFM cross-sectional traces taken along the [110] direction, we measured that the pit A lateral facets form an angle of 4.3±0.6° respect to the (001) surface. Pit B develops from pit A changing the side base orientation and this change is accomplished by a

modification of the lateral facet angle. Thus the bottom of pit B has the same facet orientation of pit A and the new facets appearing after the pit transition form an angle of 25±4°. The measured facet angles indicate that the pit A internal surfaces are vicinal Si(001) surfaces and the pit B lateral facets belong to {113} planes.

In Fig.3 (a) and (b) we report the Si/Ge fluorescence intensity ratio obtained during the X-ray scans of pit A and B, respectively. The XSM measurements were carried out at the European Synchrotron Radiation Facility on the X-ray Microscopy beamline ID21. In the experimental set-up, the synchrotron source was demagnified by a Fresnel zone plate [15] setting the energy of the incident photon beam at 2.5 keV. The X-ray lens was coherently illuminated and the size of the probe was merely determined by the zone-plate parameters obtaining a spatial resolution of about 200 nm in both directions [16]. The Si $K_{\alpha,\beta}$ and Ge $L_{\alpha,\beta}$ X-ray fluorescence emissions were collected using an energy dispersive 30 mm^2 high-purity Ge detector (Princeton Gamma-Tech) mounted in the horizontal plane perpendicular to the incident beam to minimize the contribution of elastically scattered primary X-rays. The sample was inclined towards the detector (~15°) to allow the fluorescence signals to enter the detector with a collection solid angle of about 0.6% of 4π steradians. For SiGe alloy with a 19% Ge content, the sample depth probed by the incident beam is approximately 2.2 μm whereas the escape depths of the Si and Ge fluorescence photons are 1.2 and 3 μm, respectively. From fluorescence data it is, in principle, possible to determine the absolute values of the alloy Ge concentration by taking into account: (*i*) self-absorption contributions; (*ii*) the difference in the fluorescence yields and (*iii*) the effects of the variation of the incidence and detection angles during the pit scan. The numerical determination of these corrections is difficult and is beyond the intent of this paper. An estimate of these terms following Refs. 17 and 18 shows that they modify the Si/Ge fluorescence ratio as a function of position in a monotonic way. Thus these correction terms are expected to affect only numerically the intensity without introducing any additional structure in the collected spectra. As for the AFM measurements, the X-ray scans were taken along the [110] sample direction. The integration time was 60 s/point and the samples were probed using 6 points per micron. In this way we obtained a good signal-to-noise ratio, a continuous probe of the sample surface and a minimization of the effects due to X-ray beam point instabilities. The scans start and end in the flat region close to the pit border. We found that the fluorescence curves from Si and Ge are featureless, demonstrating that the measurements are not affected

from pit geometry and shape. The ratios obtained from Si and Ge fluorescence curves are shown in Fig. 3 (a) and (b) for pit A and B, respectively. A comparison of Fig.3 (a) with the AFM image of pit A reported in Fig.2 shows that the sample region where the Si concentration increases overlaps the pit internal facets. However the measured variation of the Si concentration is consistent with the expected increase of the Si/Ge ratio due to the signals collected inside the pit deriving from the SiGe layers at lower concentration that form the graded part of the VS. The 4.3% variation of the Si/Ge ratio of Fig.3 (a) is in agreement with the calculated variation of 5% obtained following the Ref. 17 and neglecting the absorption of the Ge fluorescence from Si atoms within the detection solid angle. The XSM analysis of pit B shown in Fig.3 (b) presents a variation of the Si/Ge ratio with the scanning coordinate that is compatible with the pit profile as measured by AFM. Respect to Fig.3 (a), Fig.3 (b) exhibits two peaks for the Si/Ge ratio located at 13 and 20 μm that extend over a 2 μm wide region. To facilitate the reading of Fig. 3 (b), we identified three characteristic regions of the spectrum: (i) the flat region outside the pit and the lateral {113} oriented pit facets, labeled as I; (ii) the zone inside the bottom of the pit corresponding to the {001} vicinal facets, labeled as II, and (iii), finally, two peaks present at the border between regions I and II, labeled as III. As discussed for the case of pit A, the difference in the Si/Ge ratio between the regions I and II is due to the probing of the underlying SiGe alloy films below the epilayer at fixed Ge concentration. Here the 12% variation of the Si/Ge ratio is larger than that one observed in the previous case of Fig.3(a), because pit B is four times deeper than pit A (see Fig.2). As a consequence, the probing of the bottom region of pit B is affected by the underlying layers at variable Ge concentration in a larger percentage. In the present case the calculated variation of the Si/Ge ratio is 16%. The regions III of Fig.3 (b) represent relatively narrow Si-rich zones: the comparison of the spectrum with the AFM pit shape shows that these Si-rich zones are located at the border of the pit bottom. Moreover the values of Si/Ge ratio in regions III are well above the measured values in both the regions I and II. As a consequence we can affirm that the two peaks present in the Fig.3 (b) univocally identify sample zones in which a compositional variation of the SiGe alloy occurred.

The physical origins of pit formation during the growth of thick SiGe alloys is not well understood. Only for deep cuspidal pits, not discussed here, it seems to be accepted that they are originated from roughness and contamination at the Si wafer/Si buffer interface [11,13]. Concerning the pits analyzed in this paper, their formation during the growth, even when the growth front is some microns away from the Si/SiGe

interface, suggests that the pit formation is related to a magnification and diffusion of stress field from the Si buffer layer to the SiGe alloy. It is well established that in heterostructures, deviations from a planar growth are related to the need of strain relaxation through the formation of 3D structures [19,20]. Recently a strain driven mechanism has been demonstrated for pit evolution and some common features as the change of shape and of the facet angles can be identified in the evolution mechanism of self-organized pits and islands [13,20]. Moreover the study of the cross-hatch pattern homogeneously present on the SiGe alloy surface gives more insight on pit formation. The presence of cross-hatch pattern on SiGe surfaces is associated to a local variation of strain field that shows preferential relaxation along the [110] crystallographic directions [10,21,22]. From AFM measurements we observed that the rise of the pit is always accomplished with the break of the cross-hatch pattern lines. Furthermore the cross-hatch pattern is absent on the pit facets. This observation suggests that at the beginning of pit formation the strain stops to relieve via the cross-hatch pattern preferring the relaxation through the defect evolution. On the other hand, XSM measurements indicate that the strain-related mechanism of pit formation is not connected to local variations of the Ge concentration in the alloy. This is confirmed from the XSM analysis performed on both pit A and B: the comparison between the measured variation of the Si/Ge ratios and the calculated values show a good agreement in spite of the difficulty in estimating the parameters involved in the calculation. Pit A is homogeneous in composition and this proves that, once the pit rises, its lateral facets represent real no-growth fronts that expand along the [100] directions. When pit A evolves into pit B, the no-growth edges become parallel to the [110] directions and the pit evolution proceeds without filling the pit bottom. XSM measurements on pit B show a strong compositional variation, with Si-rich regions localized where {113} lateral pit facets are inserted. These are exactly the regions where the no-growth fronts changed directions. In analogy with the case of self-organized Ge islands on Si(001) where the island base is a stronger strain region, we expect, for the pits, a larger stress concentration at the pit bottom where the {113} lateral facets are generated. Indeed, the insertion of these facets originates zones where the lattice is compressed as compared to the neighboring regions, i.e. the vicinal (001) surfaces. In these zones (the regions III in Fig.3 (b)) we effectively observed a Si-richer alloy because the growth of a material with lower lattice parameter is preferred.

In conclusion we have demonstrated that XSM is a powerful tool able to detect spatial Ge variation in SiGe alloys with a sub-micron resolution. In particular when defects are present in VS's, XSM revealed Ge content variations in the alloy demonstrating that defects formation and evolution represent a strain relief mechanism The observed large stress concentration inside the defect and the absence of the cross-hatch pattern on its internal facets are findings in close analogy with the lateral strain relaxation of self-organized islands in heterostructures.

Fig.1

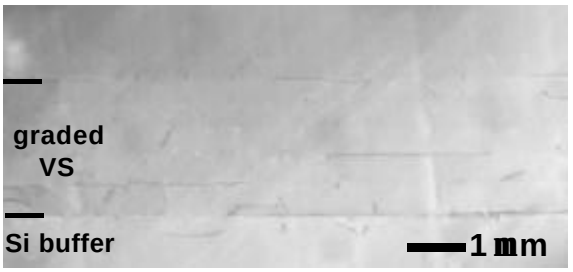

Fig. 2

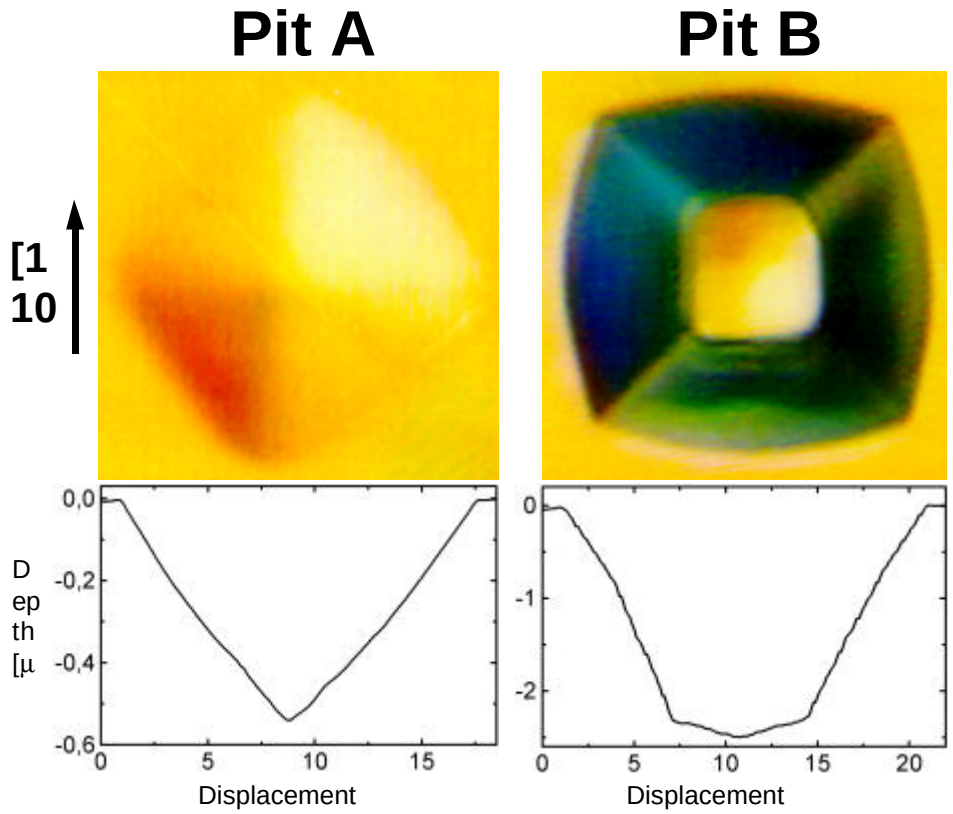
Pit A
Pit B
[1
10
D
ep
th
[µ
0,0
-0,2
-0,4
-0,6
0
5
10
15
Displacement
0
-1
-2
0
5
10
15
20
Displacement

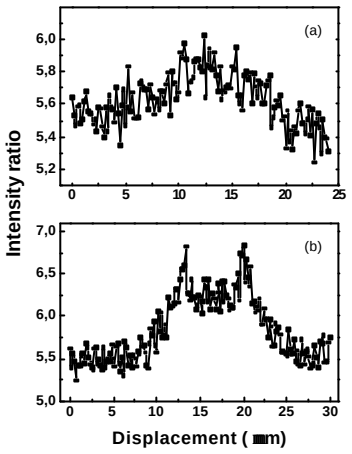

Fig. 3

References

[1] M. T. Currie, S. B. Samavedam, T. A. Langdo, C. W. Leitz, and E. A. Fitzgerald, Appl. Phys. Lett. **72**, 1718 (1998).

[2] H.-C. Luan, D. R. Lim, K. K. Lee, K. M. Chen, J. G. Sandland, K. Wada, and L. C. Kimerling, Appl. Phys. Lett. **75**, 2909 (1999).

[3] L. M. Giovane, H. C. Luan, A. M. Agarwal, and L. C. Kimerling, Appl. Phys. Lett. **78**, 541 (2001).

[4] K. Ismail, B. S. Meyerson, and P. J. Wang, Appl. Phys. Lett. **58**, 2117 (1991).

[5] G. Schuberth , F. Schäffler, M. Besson, G. Abstreiter, and E. Gornik, Appl. Phys. Lett. **59**, 3318 (1991).

[6] F. Schäffler, D. Többen, H. J. Herzog, G. Abstreiter, and B. Holländer, Semicond. Sci. Technol. **7**, 260 (1992).

[7] F. Schäffler, Semicond. Sci. Technol. **12**, 1515 (1997).

[8] N. Sugii, K. Nakagawa, Y. Kimura, S. Yamaguchi, and M. Miyao, Semicond. Sci. Technol. **13**, A140 (1998).

[9] A. C. Churchill, D. J. Robbins, D. J. Wallis, N. Griffin, D. J. Paul, A. J. Pidduck, W. Y. Leong, and G. M. Williams, J. Vac. Sci. Technol. **B 16**, 1634 (1998).

[10] P. J. McNally, G. Dilliway, J. M. Bonar, A. Willoughby, T. Tuomi, R. Rantamäki, A. N. Danilewsky, D. Lowney, Appl. Phys. Lett. **77**, 1644 (2000).

[11] S. Kanjanachuchai, T. J. Thornton, J. M. Fernández, and H. Ahmed, Semicond. Sci. Technol. **13**, 1215 (1998).

[12] K. M. Chen, D. E. Pesson, and S. J. Pennycook, Appl. Phys. Lett. **66**, 34 (1995).

[13] L. Di Gaspare, E. Palange, G. Capellini, and F. Evangelisti, J. Appl. Phys. **88** 120 (2000).

[14] L. Di Gaspare, K. Alfaramawi, F. Evangelisti, E. Palange, G. Barucca, and G. Majni, Appl. Phys. Lett. **79**, 2031 (2001).

[15] J. Susini, R. Barrett, B. Kaulich, S. Oestreich, M. Salomé, Proceedings of the 6th International Conference on X-ray microscopy, Berkeley, 1999, W. Meyer-Ilse, T. Warwick, and D. Attwood (eds.), AIP Conference Proceedings **507**, 19 (2000).

[16] C. David, B. Kaulich, R. Barrett, M. Salomé, and J. Susini, Appl. Phys. Lett. **77**, 3851 (2000).

[17] Z. Tan, J. I. Budnick, and S. M. Heald, Rev. Sci. Instrum. **60**, 1021 (1989).

[18] L. Tröger, D. Arvanitis, K. Baberschke, H. Michaelis, U. Grimm, and E. Zschech, Phys. Rev. B **46**, 3283 (1992).

[19] J. Tersoff, and F. LeGoues, Phys. Rev. Lett. **72**, 3570 (1994).

[20] A. L. Barabasi, Appl. Phys. Lett. 70, 2565 (1997).

[21] E. A. Fitzgerald, Y.-H. Xie, D. Monroe, P. J. Silverman, J. M. Kuo, A. R. Kortan, F. A. Thiel, and B. E. Weir, J. Vac. Sci. Technol B **10**, 1807 (1992).

[22] M. H. Gray, J. W. P. Hsu, L. Giovane, and M. T. Bulsara, Phys. Rev. Lett. **86**, 3598 (2001).

Figures captions

Fig. 1. Cross section transmission electron microscopy of a typical virtual substrate is shown. Markers indicate the graded region and only a partial view of the top layer at fixed concentration is reported.

Fig. 2. Optical microscope images and atomic force microscopy profiles (a) of pits A and (b) of pit B, are shown.

Fig. 3. X-ray scanning microscope Si/Ge fluorescence ratio, (a) for pit A and (b) for pit B, are reported.

The paper has been submitted to Applied Physics Letters for publication